

Northumbria Research Link

Citation: Petersen, Lene, Pellicciotti, Francesca, Juszak, Inge, Carengo, Marco and Brock, Benjamin (2013) Suitability of a constant air temperature lapse rate over an Alpine glacier: testing the Greuell and Böhm model as an alternative. *Annals of Glaciology*, 54 (63). pp. 120-130. ISSN 02603055

Published by: Publishing Technology

URL: <http://dx.doi.org/10.3189/2013AoG63A477>
<<http://dx.doi.org/10.3189/2013AoG63A477>>

This version was downloaded from Northumbria Research Link:
<https://nrl.northumbria.ac.uk/id/eprint/13771/>

Northumbria University has developed Northumbria Research Link (NRL) to enable users to access the University's research output. Copyright © and moral rights for items on NRL are retained by the individual author(s) and/or other copyright owners. Single copies of full items can be reproduced, displayed or performed, and given to third parties in any format or medium for personal research or study, educational, or not-for-profit purposes without prior permission or charge, provided the authors, title and full bibliographic details are given, as well as a hyperlink and/or URL to the original metadata page. The content must not be changed in any way. Full items must not be sold commercially in any format or medium without formal permission of the copyright holder. The full policy is available online: <http://nrl.northumbria.ac.uk/policies.html>

This document may differ from the final, published version of the research and has been made available online in accordance with publisher policies. To read and/or cite from the published version of the research, please visit the publisher's website (a subscription may be required.)

Suitability of a constant air temperature lapse rate over an Alpine glacier: testing the Greuell and Böhm model as an alternative

Lene PETERSEN,¹ Francesca PELLICCIOTTI,¹ Inge JUSZAK,¹ Marco
CARENZO,¹ Ben BROCK,²

¹*Institute of Environmental Engineering, ETH Zurich, Zurich, Switzerland*

E-mail: petersen@ifu.baug.ethz.ch

²*School of the Built and Natural Environment, Northumbria University, Newcastle Upon Tyne NE1 8ST, UK*

ABSTRACT. Near surface air temperature, typically measured at a height of 2 m, is the most important control on the melt rate at a snow or ice surface. It is distributed in an overly-simplistic manner in most glacier melt models by using constant linear lapse rates, which poorly represent the actual spatial and temporal variability of air temperature. In this study we test a simple thermodynamic model proposed by Greuell and Böhm in 1998 as an alternative, using a new data set of air temperature measurements from along the flowline of Haut Glacier d’Arolla, Switzerland. The unmodified model performs little better than assuming a constant linear lapse rate. When modified to allow the ratio of the boundary layer height to the bulk heat transfer coefficient to vary along the flowline, the model matches measured air temperatures better and a further reduction of the Root Mean Square Error is obtained, although there is still considerable scope for improvement. The modified model is shown to perform best under conditions favourable to the development of katabatic winds: few clouds, positive ambient air temperature, limited influence of synoptic or valley winds and a long fetch, but its performance is poor under cloudy conditions.

23 1. INTRODUCTION

24 Near surface temperature, T_a , typically measured at a height of 2 m, is the most important control on the energy exchange and
25 melt rate at a snow or ice surface. For spatially distributed glacier melt modelling a distributed temperature input is needed,
26 which is normally generated by extrapolation from point measurements with a linear lapse rate (LR). The LR describes the
27 dependency of temperature with elevation and is considered to be positive when temperature increases with elevation (e.g.
28 Minder and others, 2010). A steep (strongly negative) LR indicates a fast decrease of temperature with increasing altitude
29 (see e.g. Pepin and Losleben, 2002). In most glacier melt models, the temperature is represented with a constant in time
30 and uniform in space LR (e.g. Klok and Oerlemans, 2002; Hock and Holmgren, 2005; Machguth and others, 2006; Huss and
31 others, 2008; Farinotti and others, 2012). Generally such a LR lies between -0.0055 and -0.0065 °C/m (e.g. Arnold and others,
32 2006; Machguth and others, 2006; Michlmayr and others, 2008; Gardner and Sharp, 2009; Paul and others, 2009; Nolin and
33 others, 2010), the latter often being referred to as the Environmental Lapse Rate (ELR) (or mean Moist Adiabatic Lapse
34 Rate (MALR)). Both the assumption of a constant in time and uniform in space LR, and the use of the ELR have been
35 recently questioned for high elevation and glacierised basins. Most studies on the variability of near-surface temperature LRs
36 over glaciers have found generally lower LRs than the ones commonly used (e.g. Strasser and others, 2004; Li and Williams,
37 2008; Hulth and others, 2010), while Minder and others (2010) pointed out that there is no physical basis for the use of the
38 ELR in high elevation basins where the effect of the terrain cannot be neglected. Spatio-temporal patterns of air temperature
39 variability have been shown to be affected by various factors of the surface environment and atmospheric conditions (see
40 Marshall and others, 2007), so that the application of free atmosphere LRs is questionable. Temporal variability has been
41 shown to be important at all scales in various studies (e.g. Stahl and others, 2006; Marshall and others, 2007; Gardner and
42 others, 2009; Chutko and Lamoureux, 2009; Petersen and Pellicciotti, 2011), while spatial variations are more complex than
43 the simple linear dependency with elevation assumes (e.g. Strasser and others, 2004; Brock and others, 2010; Petersen and
44 Pellicciotti, 2011). An additional limitation of to the use of a constant LR to extrapolate air temperature from off-glacier
45 stations is that changes in temperature off-glaciers are in general higher than on-glacier because of the dampening effect of the
46 glacier (Greuell and Böhm, 1998). This effect cannot be taken into account by use of a simple LR and the higher temperature
47 changes would be translated as such onto the glacier surface.

48 Lack of extensive T_a data sets on glaciers is a key restriction for a thorough analysis of temperature variability in space and
49 time, as well as for development of models. Using a high resolution data set of temperature time series at several locations
50 along the glacier flowline of Juncal Norte Glacier, Chile, Petersen and Pellicciotti (2011) found a strong diurnal LR cycle
51 driven by the development of a katabatic boundary layer (KBL), with steeper LRs in the afternoon when katabatic wind was
52 eroded and elevation was reestablished as the main control of air temperature variability. A KBL develops on melting glaciers

53 when the air temperature above the glacier, which is normally higher than that of the glacier surface (which cannot exceed
54 0°C), is cooled by the surface. The cooling increases its density and the resulting density gradient produces katabatic flow (e.g.
55 Ohata, 1989; Greuell and others, 1997; Klok and others, 2005; Pellicciotti and others, 2008). Most studies using procedures to
56 generate temperature fields to drive melt models do not account for processes within the KBL (Shea and Moore, 2010) even
57 though it is a main control over temperature variability. The presence of the KBL affects the thermal regime by reinforcing
58 the turbulent exchange of heat by sensible fluxes and the cooling of the air adjacent to the surface. As a result, temperatures
59 within the KBL are cooler than those outside (Greuell and Böhm, 1998; Marshall and others, 2007; Shea and Moore, 2010).
60 Empirical approaches to take into account the difference in regime between on and off-glacier temperature have been suggested
61 by Shea and Moore (2010) and Braithwaite and others (2002). An attempt to include these effects was proposed by Greuell
62 and Böhm (1998) with a thermodynamic model (henceforth referred to as GB98) in which air temperature is derived as a
63 function of slope and distance along the flowline. This approach was suggested as variations in air temperature along the valley
64 glacier Pasterze Glacier, Austria, could not be explained by means of a constant LR (see section 4). GB98 is, to our knowledge,
65 the only model of air temperature distribution on glaciers that has been suggested as a realistic and practical alternative to
66 extrapolation using LRs. However, there has been little published work applying the model to other glaciers or testing its
67 main assumptions. The aim of this paper is therefore to investigate the suitability of the GB98 model for calculation of air
68 temperature distribution across a well studied alpine glacier, Haut Glacier d’Arolla (HGdA, see Figure 1), in the Swiss Alps,
69 and to explore its strengths and limitations in comparison with the commonly used LR approach. For this, we make use of a
70 new data set of distributed temperature records collected on HGdA during the 2010 ablation season.

71 **2. EXPERIMENTAL SETUP**

72 Our study site is HGdA, in the Val d’Hérens in southern Switzerland (Figure 1a). It has an area of 4 km^2 and a length of 4 km
73 and comprises two basins feeding a tongue. The elevation ranges from 2590 m to about 3500 m with a generally constant and
74 gentle slope (see Figure 1b). About 36 % of the basin is glacierised. Numerous studies of glacier energy balance and ablation,
75 meteorology and hydrology have been conducted on the glacier (e.g. Nienow and others, 1996; Arnold and others, 1996; Willis
76 and others, 2002; Pellicciotti and others, 2005; Brock and others, 2006; Carenzo and others, 2009).

77 In 2010, a glacio-meteorological field campaign was conducted from 24th of May until the 12th of September. The setup
78 included 5 Automatic Weather Stations (AWSs) and 7 T-Loggers used in this study (see Figure 1a). The AWSs measured at
79 a 5-second interval and stored averaged 5-minute records of air temperature ($^{\circ}\text{C}$), relative humidity (%), wind speed (ms^{-1}),
80 wind direction ($^{\circ}$), and incoming and reflected shortwave radiation (Wm^{-2}). The thermometers of AWS2, AWS3 and AWS4
81 were ventilated and shielded, while AWS1 and AWS5 were shielded but not ventilated. The T-Loggers consisted of a HOBO
82 TidbiT v2 UTBI-001 temperature sensor with integrated datalogger housed in a shielded PVC cylinder and fixed to a metal

83 tripod 2 m above the surface. The details of this setup are described in Petersen and Pellicciotti (2011). The T-Loggers used in
 84 this study were located along the glacier flowline, some of them close to the AWSs (Figure 1a). They measured at an interval
 85 of 5 or 10 minutes. All data were aggregated to hourly values for the analysis. The characteristics of the AWSs and T-Loggers
 86 are listed in Table 1. In this work, we mainly use the temperature data from the T-Loggers for the analysis of the temporal and
 87 spatial variability of 2 m air temperature and testing of the model, and the data from the AWSs for analysis of wind direction
 88 and derivation of cloud transmittance factors. We also use data measured at two permanent off-glacier stations, AWS-T1
 89 and AWS-T2 (Figure 1a). AWS-T1 is located on rock near the glacier terminus at an elevation of 2500 m. AWS-T2 is set up
 90 on periglacial debris of the easterly slopes next to the glacier at an elevation of 2990 m. Longwave radiation (Wm^{-2}) and
 91 temperature ($^{\circ}\text{C}$) from the two off-glacier AWSs are used for the calculation of cloud cover and the corresponding classification
 92 in cloud classes (Section 5). The temperature record of AWS-T2 provides the input to the model. Some of the T-Loggers fell
 93 down on the glacier surface during certain periods which were therefore excluded. For the analysis we use only the data when
 94 all T-Loggers were functioning, so that the data set consists of 1284 hours of non-continuous measurements. TL6 was not
 95 considered in the analysis due to a very short functioning period. This common period (indicated by the grey bar in Figure
 96 4) is used to compute the main statistics for the temperature series at each T-Logger (Table 1). An airborne LiDAR (Light
 97 Detection And Ranging) flight over the HGdA glacier basin in October 2010 by Helimap System SA provided a DEM (Digital
 98 Elevation Model) with a grid resolution of 10 m, which is used as the basis of the model in this paper, in particular to derive
 99 the glacier slope and the distance along the flowline (see Figure 1 for details). The elevations of the AWSs and T-Loggers were
 100 measured with differential GPS.

101 3. APPLICATION OF A CONSTANT LAPSE RATE (CLR)

102 We calculated a constant in time and uniform in space LR using the data from the T-Loggers, as well as a LR variable in time,
 103 to test the validity of the commonly used method of T_a extrapolation on HGdA. The data show high temporal variability on
 104 different scales as well as spatial variations across the glacier (Figure 2a). The figure shows the lapse rate calculated through
 105 linear regression using i) all T-Loggers, ii) all T-Loggers in the lower part of the glacier (TL7, TL8, TL9) and iii) all T-Loggers
 106 in the upper part (TL1, TL2, TL3). The differences at both spatial and temporal scale are significant. The lower section of the
 107 glacier is characterized by steep, negative LRs while the upper section has less negative LRs or even positive ones, indicating
 108 inversions. Use of one single variable LR for the entire glacier averages out the two behaviors, also reducing the observed
 109 temporal variability. If the LR is also averaged in time over the season, we obtain an unrealistic value that only results from
 110 compensation of contrasting patterns. It is thus evident that application of a constant LR would not represent the actual
 111 temperature variability over the glacier, in time nor space. Figure 2b shows the comparison of observed temperature with
 112 temperature extrapolated from AWS-T2 with the ELR ($-0.0065 \text{ }^{\circ}\text{Cm}^{-1}$) and a calibrated constant LR (CLRcal). Previous

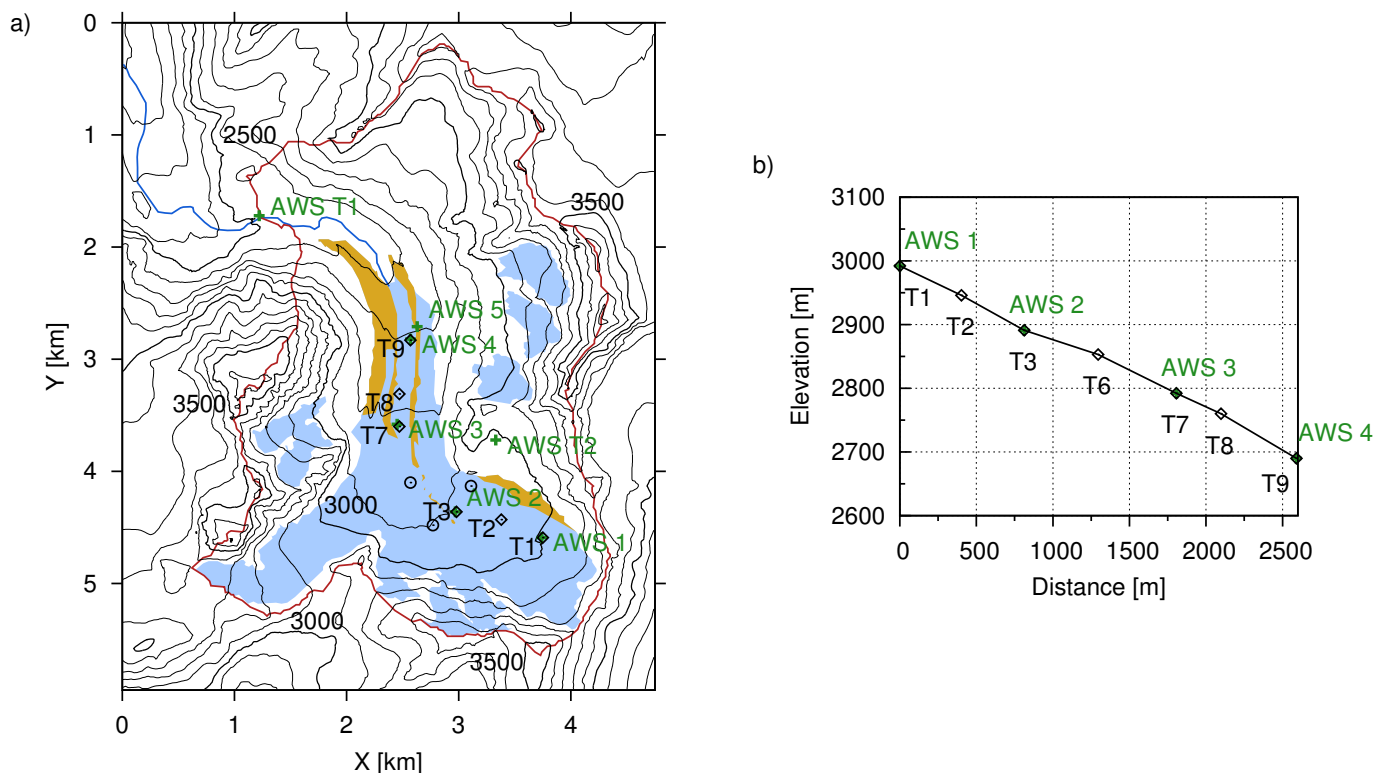


Fig. 1. a) Map of Haut Glacier d'Arolla showing the glacierised area (blue), the debris covered area (brown) and the catchment outline (red). Green '+' indicates the locations of AWS in 2010, 'o' indicates the positions of T-loggers which are not used in the analysis; the T-loggers along the flowline are indicated with diamonds and labeled. The upper left corner of the plot is 604030, 94910 in Swiss coordinates. b) Surface profile along the flowline. AWS5 is approximately at the same elevation as AWS4.

113 to the extrapolation, data at AWS-T2 were corrected. A systematic difference between the temperature data at AWS-T2 and
 114 at the uppermost T-Logger TL1 is evident (Table 2). Although the two stations are at almost the same elevation, the mean
 115 temperature over the common period is about 0.5 °C colder at AWS-T2 than at the location on the glacier (Table 2). This
 116 effect might be due to the location of AWS-T2 being windier and to the air being better mixed. It could also be caused by
 117 differences in the ventilation of the sensors as well as by the fact that the boundary layer at TL1 might be thin and thus the
 118 station might measure outside of the GBL. However, the exact cause cannot be identified precisely given the limited amount
 119 of data available. To exclude this systematic error, we corrected the temperature at AWS-T2 with an offset of 0.5 °C. The
 120 constant LR was calibrated by minimizing the Root Mean Square Error (RMSE) at all T-Logger locations over the whole time
 121 series for the common period of record. The CLRcal is equal to $-0.0032\text{ }^{\circ}\text{Cm}^{-1}$ and thus shallower than the ELR, confirming
 122 evidence from previous studies (e.g. Marshall and Sharp, 2008; Shea and Moore, 2010). Use of an ad hoc calibrated LR provides
 123 an obvious improvement over the use of the standard ELR (Figure 2b).

Table 1. Characteristics of the AWSs and T-Loggers: name, elevation, X-Coordinate, Y-Coordinate, mean temperature and standard deviation (std). Mean temperature and standard deviation are calculated over the common period of record (1284 hours) unless stated otherwise. The elevation and coordinates of the AWSs and T-Loggers were measured with a differential GPS. *over bare ground. **not ventilated. ***only measuring the first weeks during a relatively cold period.

Name	Elevation (m)	X-Coordinate (m)	Y-Coordinate (m)	Mean Temp. (°C)	Std Temp (°C)
AWS-T1*	2500	605248	93193	5.86	4.28
AWS-T2*	2990	607356	91193	2.87	4.21
AWS1**	2992	607766	90330	3.10	4.00
AWS2***	2890	606987	90560	1.21	3.19
AWS3	2797	606489	91326	3.04	3.27
AWS4	2680	606588	92097	5.04	4.17
AWS5**	2662	606655	92207	4.61	3.84
TL1	2992	607766	90330	3.36	3.94
TL2	2946	607407	90482	3.53	3.82
TL3	2891	606987	90560	3.44	3.61
TL6***	2853	606594	90814	(2.11)	(3.52)
TL7	2792	606489	91326	3.75	3.38
TL8	2760	606576	91609	4.00	3.43
TL9	2680	606588	92050	4.75	3.78

124 4. APPLICATION OF THE GREUELL AND BÖHM MODEL (GB98)

125 In the description of the GB98 model we follow the naming convention of the original paper. The main assumption of this
126 simple thermodynamic model is that temperature distribution over a melting glacier is a balance between adiabatic warming
127 (cooling) due to compression (expansion) of air moving along the glacier and the sensible heat exchange with the underlying
128 ice surface (see van den Broeke, 1997). Hence, air temperature distribution is parameterized as mainly a function of slope and
129 along-glacier distance. Temperature changes due to surrounding topography, entrainment, phase changes, radiation divergence
130 and variation of fluxes in the horizontal direction are neglected. These assumptions were based on results obtained by van
131 den Broeke (1997) on Pasterze glacier during the 1994 summer season. The author argued from analysis of wind directions
132 that conditions on Pasterze were mostly dominated by the katabatic or glacier wind. The model is based on a number of
133 other simplifying assumptions, such as that the height of the glacier wind layer (H) and the glacier slope are constant. These

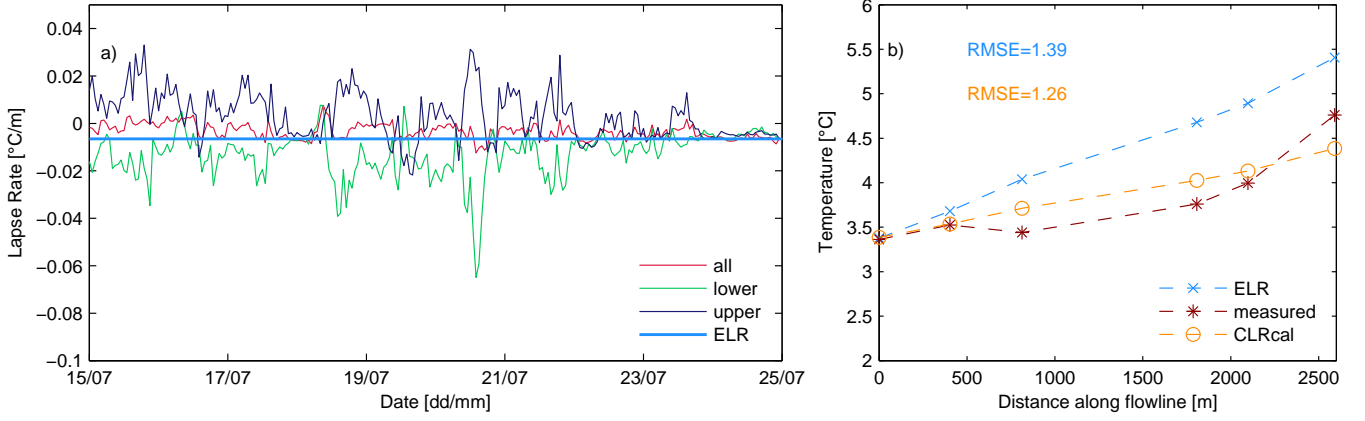


Fig. 2. a) Comparison of the constant ELR with LR's variable in space and time: regression of all T-Loggers along the flowline (TL1,TL2,TL3,TL7,TL8,TL9) (indicated with "all"); upper LR (indicated by "upper") obtained from regression of the upper T-Loggers (TL1,TL2 and TL3) and lower LR (indicated by "lower") obtained from regression of the lower T-Loggers (TL7, TL8 and TL9). b) Comparison of mean observed temperature at each T-Logger with temperature extrapolated from AWS-T2 with the ELR and the calibrated constant LR (CLRcal). Also indicated is the Root Mean Square Error (RMSE) for the two model versions.

134 assumptions were discussed by Greuell and Böhm (1998) for the Pasterze Glacier and will be addressed in the following
 135 section. Since the model is based on the hypothesis that the glacier wind is present, a requirement for its application is an air
 136 temperature greater than the surface temperature so that the glacier wind is likely to develop (see Section 1).

137 For the application of the model, the glacier geometry must be known in order to derive slope angle and distance along
 138 the glacier flowline. This information can be extracted from glacier DEMs that can also be provided by downloadable
 139 global databases, e.g. glacier outlines from the World Glacier Monitoring Service/Global Land Ice Measurements from Space
 140 (WGMS/GLIMS) and DEMs from the Shuttle Radar Topography Mission (SRTM), which makes the model appealing in terms
 141 of applicability. We used the DEM described in Section 2 above. Here we report only the main equations of the model and
 142 refer the reader to the original paper by Greuell and Böhm (1998) for more details. The potential temperature Θ is calculated
 143 as

$$\Theta(x) = (T_0 - T_{eq}) \exp\left(-\frac{x - x_0}{L_R}\right) - b(x + x_0) + T_{eq} \quad (1)$$

144 From this, the actual temperature can be derived as:

$$T(x) = (T_0 - T_{eq}) \exp\left(-\frac{x - x_0}{L_R}\right) + T_{eq} \quad (2)$$

145 with:

$$T_0 = T_{cs} - \gamma(z_{cs} - z_0) \quad (3)$$

$$T_{eq} = b L_R \quad (4)$$

$$b = \Gamma \tan(\alpha) \quad (5)$$

$$L_R = \frac{H \cos(\alpha)}{c_H} \quad (6)$$

146 where $T(x)$ is the temperature at a distance x along the glacier flowline, T_0 the temperature at $x=0$, T_{eq} the equilibrium
 147 temperature value, Γ the dry adiabatic LR ($-0.0098 \text{ }^\circ\text{Cm}^{-1}$), c_H the bulk transfer coefficient for heat (see Stull (1988)) and
 148 T_{cs} and z_{cs} are the temperature and elevation of the climate station outside of the glacier's influence used to drive the model
 149 (AWS-T2 in our study). All equations above are based on the assumptions that the glacier slope is constant and that the ratio
 150 H/c_H is constant along the flowline.

151 The equations above contain five unknown parameters: x_0 and z_0 , the location and elevation where the air parcel enters the
 152 layer influenced by the glacier, the length scale L_R and b (which are defined above and depend on the glacier slope (α)) and
 153 γ , the lapse rate used to extrapolate temperature from the input climate station (T_{cs}) to the initial point (x_0, z_0). Here we
 154 apply the model to the entire data set of temperature observations (common period of record), following the same approach as
 155 Greuell and Böhm (1998). We use the same values of γ ($-0.007 \text{ }^\circ\text{Cm}^{-1}$), H (equal to 17 m as estimated for Pasterze by Greuell
 156 and Böhm (1998)) and c_H (0.002 following Stull (1988)) as used by the authors. We refer to this setup as the unmodified
 157 model, but test different assumptions for the position and elevation of the uppermost point of the flowline (x_0 and z_0), as
 158 recommended by GB98, who pointed to the fact that both x_0 and z_0 could be regarded as tuning parameters. The best fit
 159 is obtained by assuming the uppermost T-Logger (TL1) as the initial point (of coordinate x_0 and elevation z_0 , respectively).
 160 Model sensitivity was then analysed by varying the other parameters by $\pm 10, 25$ and 50% around the initial values taken
 161 from Greuell and Böhm (1998). Variations in H (constant along the flowline), the slope (and thus b and L_R) and γ in the
 162 range above resulted in small changes in the temperature profile (not shown here). Varying γ ($\pm 10, 25$ and 50%) did not have
 163 a major effect as expected considering the similar elevation of the climate station and of the initial point (TL1) (see Table 1).
 164 We also tested the effect of using different off-glacier data as input to the model, but the differences when using the nearest
 165 MeteoSwiss station Grand St. Bernard (2472 m, 579137/79856 m, located at a distance of 30.4 km) were negligible.

166 Figure 3a shows the comparison of measured air temperature with air temperature extrapolated with the calibrated constant
 167 LR (CLRcal) and modelled with the GB98 model, for the common period of record. Even though the CLRcal seems to work
 168 in an acceptable manner, the RMSE is reduced by 7% by applying the GB98. The CLRcal leads to underestimation of

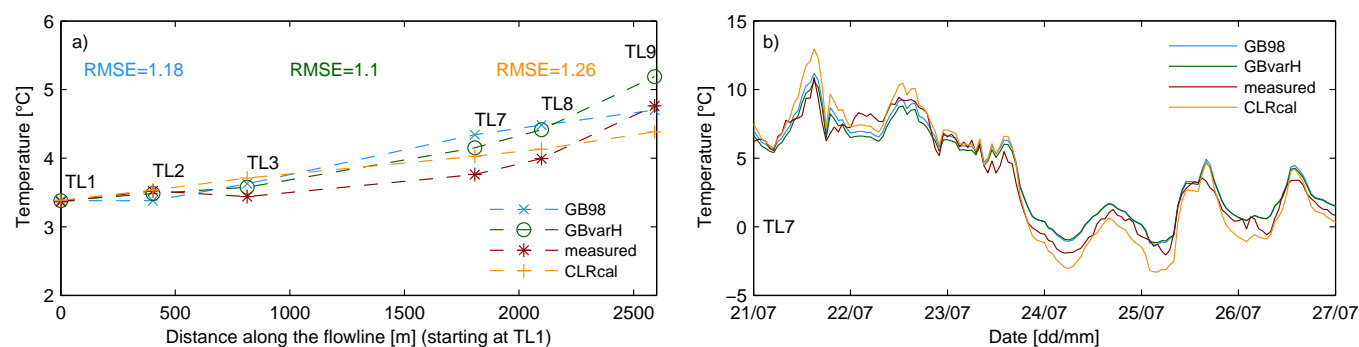


Fig. 3. Comparison of observed temperature and temperature modelled with the GB98 with the values of H , γ and Γ suggested in the original paper for Pasterze glacier (GB98, referred to in the text as unmodified model) and the modified version (GBvarH, Section 5): a) average values along the flowline; and b) time series at TL7 for a selected sub-period (21 to 27 of July).

169 temperatures during cold periods and overestimation during warm periods (Figure 3b). As these two errors compensate each
 170 other, the net effect is an apparent good performance if we look only at the average values over the season (Figure 3a).

171 The GB98 on average overestimates temperature in the central part of the glacier (TL3, TL7 and TL8). The observations
 172 reveal a profile along the glacier flowline that is characterised by average temperatures decreasing more slowly in the central
 173 part of the glacier than in the uppermost and lower sections (Figure 3b). This profile cannot be reproduced by the model,
 174 which exhibits a more linear change in air temperature with distance along the flowline than is observed.

175 5. APPLICABILITY OF THE GB98 MODEL UNDER DIFFERENT 176 METEOROLOGICAL CONDITIONS

177 The results of the application of the GB98 model to the entire data set reveal that the model cannot reproduce the ob-
 178 served variability on HGdA in its original form (Figure 3), even if parameters are varied to adjust the model outputs to the
 179 observations.

180 The model is based on the assumption of two main fluxes controlling the exchange of energy at the glacier surface and
 181 affecting the temperature of air in the GBL (see Section 4), and it requires, in particular, that the glacier wind is well
 182 developed. The latter is generated by the temperature deficit between the glacier surface and overlaying air, which causes the
 183 air particles above the surface to cool down and gravitationally flow because of the associated increase in density (e.g. Stenning
 184 and others, 1981; Greuell and Böhm, 1998; van den Broeke, 1997). We therefore analysed the climatic conditions typical of
 185 the 2010 season in detail, to assess under which conditions the assumptions of the model are justified. We defined categories
 186 for air temperature, cloudiness and wind direction on a *daily* basis as follows:

187 1. *Temperature*: the temperature record was divided in two classes representative of cold and warm air temperature: i) T1,
 188 days for which more than 80% of the hourly values are above 0°C; and ii) T2, including the remaining cases. Most days
 189 fell into category T1, indicating the existence of conditions favouring the development of katabatic wind.

190 2. *Wind*: the influence of wind was investigated by defining four classes: i) W1, characterised by mainly downvalley wind
 191 (more than 80% of the hourly values); ii) W2, characterised by a diurnal cycle with mainly downvalley wind at night and
 192 in the morning hours (more than 60% of the hourly values between 21.00 and 12.00) and mainly upvalley wind in the
 193 afternoon hours (more than 60% of the hourly values between 13.00 and 20.00), which was identified as typical pattern of
 194 several days and a clear distinction from other conditions could be made; iii) W3, with a mixed wind pattern (all remaining
 195 cases); and iv) W4, with mainly upvalley wind (more than 80% of the hourly values). For this classification, we used the
 196 frequency distribution of the wind direction data from AWS4. However, the classification was compared to that obtained
 197 from the records at the other AWSs showing a nearly perfect correspondence.

198 3. *Cloud cover*: the categories for clouds were derived by classifying the days on the basis of cloud transmittance factors
 199 or cloud cover, n , derived from the measured incoming longwave radiation data at three AWSs (AWS-T1, AWS-T2 and
 200 AWS5). We adopted the approach by Marty and Philipona (2000), which is based on the comparison of the atmospheric
 201 emissivity eps_a and the potential clear-sky atmospheric emissivity eps_p (calculated with Brutsaert formula (Brutsaert,
 202 1975), for the reasons explained in Marty and Philipona (2000)). The ratio of the two emissivities provides a clear-sky
 203 index, the complement of which is the cloud factor. This method was found to be superior to methods based on the ratio
 204 of potential clear-sky to measured shortwave radiation (which are often used (Brock and Arnold, 2000)), by Juszak and
 205 Pellicciotti (2012). The cloud cover was estimated on the basis of a linear regression between eps_p and 1, where $eps_a = eps_p$
 206 corresponds to a cloud cover of zero and $eps_a = 1$ to a cloud-cover of one.

$$eps_a = \frac{lw}{\sigma T^4} \quad (7)$$

207 with T (K) being the air temperature, lw (Wm^{-2}) the measured incoming longwave radiation and σ the Stefan-Boltzmann
 208 constant. The daily cloud cover n was calculated as the mean of the hourly values at the three AWSs This value was then
 209 used to identify 4 categories: i) C1: $n > 0.8$ overcast days ; ii) C2: $0.4 < n \leq 0.8$ days with considerable cloud cover ; iii)
 210 C3: $0.1 < n \leq 0.4$ days with few clouds; and iv) C4: $n \leq 0.1$ clear-sky days.

211 The categories are listed in Table 2 and shown in Figure 4 together with the record of air temperature at AWS4. Periods
 212 of high temperatures (T1) often occur in correspondence to downvalley winds (W1) (Figure 4). In colder days, the wind

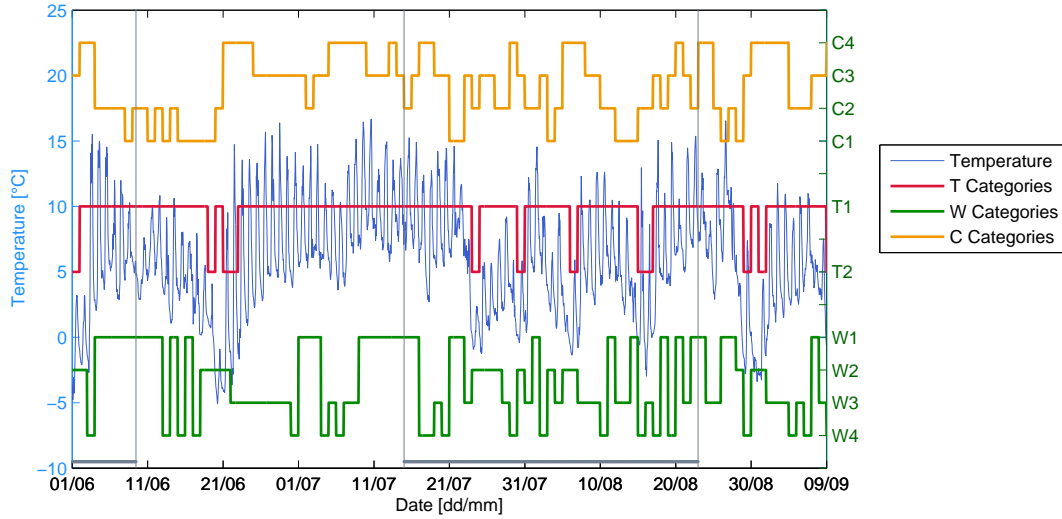


Fig. 4. Time series showing the defined conditions for cloud cover (C1 cloudy, C2 mainly cloudy, C3 partly cloudy, C4 clear-sky), temperature (T1 warm, T2 cold) and wind conditions (W1 downvalley, W2 diurnal switch downvalley/upvalley, W3 variable wind conditions, W4 upvalley) on a daily scale together with observed temperature at AWS4. The common period of observations used in the analysis is indicated by the grey bars at the bottom of the figure.

213 does not show a clear pattern but a tendency towards upvalley winds. From the temperature record, two main patterns can
 214 be observed: a first period of high temperatures (from about 21st of June to 21st of July) and a second period of colder
 215 temperature characterised by lower mean values and higher variability (from 21st of July onwards). The stable, warm period
 216 (21st of June to 21st of July) is also associated with more stable conditions for wind and cloud cover, with mostly clear sky
 217 days (C3 and C4) and wind conditions W1, W2 and W3 (i.e. no upvalley wind).

218 Assumption of a constant H over the glacier seems a limitation of the model, given that we expect the KBL to be better
 219 developed in the lower sections of the glacier. We therefore tested a model version with a variable H along the glacier flowline
 220 (GBvarH). Figure 5 shows the model results for the categories listed above for the unmodified model (GB98) described in
 221 section 4 and for the modified model (GBvarH), together with the actual temperature measurements. The values of H in
 222 correspondence of each T-Logger were found by minimizing the RMSE at each T-Logger for the time series of the common
 223 period of record. This corresponds to applying a piece-wise constant H for the different sections of the glacier, as a continuous
 224 variability of H would require knowledge of the functional dependency of H with x and the integration of the corresponding
 225 equation. Such functional dependency however cannot be inferred from the available data. The configuration resulting from
 226 the piece-wise calibration is $H = [10 \text{ m (TL2, TL3), 14 m (TL7), 16 m (TL8) and 26 m (TL9)]$.

227 A number of results are apparent from Figure 5. In most cases the application of a variable boundary layer thickness
 228 (GBvarH) is better able to represent the shape of the temperature profile along the flowline than the model assuming a
 229 constant boundary layer thickness. Under overcast conditions (C1), the model does not work well with a constant (GB98) nor

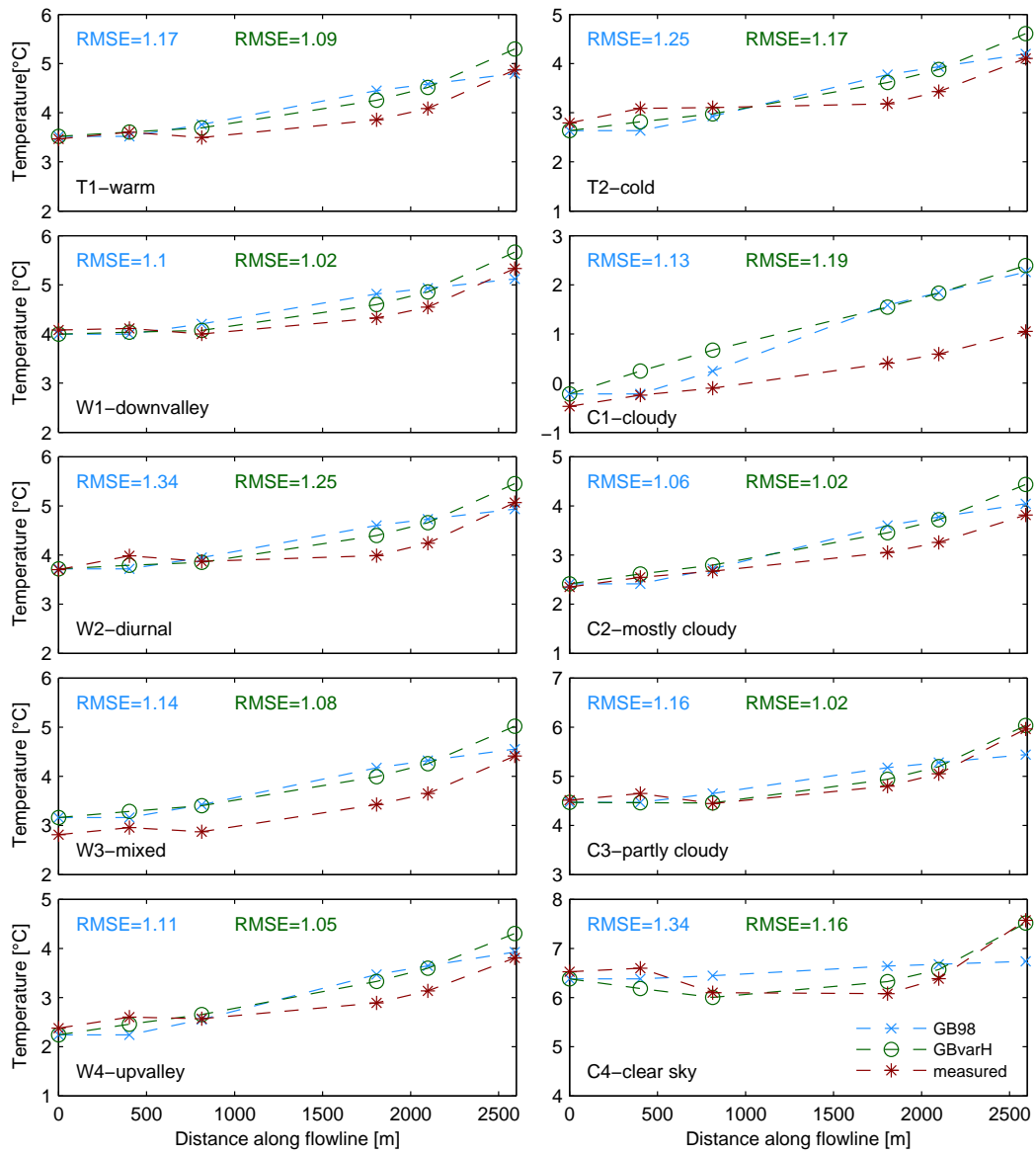


Fig. 5. Measured air temperature along the flowline in comparison with results of the unmodified model (GB98) and model with variable H (GBvarH) for the different climatic conditions described in Table 2.

Table 2. Summary of the climatic categories identified for analysis of the model results, description of criteria and the number of days corresponding to each category

ID	Explanation	Nr. of days	
		whole time series	period of common data
T1	80% of hourly temperature data are above 0°C	87	40
T2	all remaining days (cold days)	22	17
W1	at least 80% of hourly wind data in downvalley direction	37	17
W2	at least 60% of hourly wind data in the afternoon (13:00-20:00) in upvalley direction		
	at least 60% of hourly wind data during the rest of the day in downvalley direction	29	10
W3	all days with no clear wind pattern identifiable	25	15
W4	at least 80% of hourly wind measurements in upvalley direction	18	11
C1	cloudy	18	8
C2	mostly cloudy	32	19
C3	partly cloudy	32	16
C4	clear sky	27	10

230 with a variable H (GBvarH). To support the visual evaluation of model performance (Figure 5), we calculated the RMSE at
 231 each T-Loggers and the mean RMSE at all sites to quantitatively assess the model performance for the different conditions.
 232 For all conditions, the application of a variable H reduces the RMSE, except for cloudy conditions (cloud category C1) (Figure
 233 5), even though improvements are minor for some of the categories. Both model versions are able to represent the almost
 234 linear shape of temperature that corresponds to very cold (cloudy) conditions, but neither can reproduce the correct slope.
 235 For all conditions except cloudy days the model performance is highest at TL7 and TL8 (followed by TL9 and then TL2),
 236 indicating that the model works best on the lower glacier section under conditions favourable to the development of katabatic
 237 wind. The improvement allowed by varying H is stronger on the lower section of the glacier under clear-sky conditions (with
 238 a mean improvement in RMSE of 12% in the upper part and of 17% in the lower), as well as under warm temperatures and
 239 downvalley winds.

240 For downvalley wind conditions (W1) and warm temperatures (T1) the fit for the mean values is good. This is evident
 241 also from analysis of the mean diurnal cycles at different locations (Figure 6). It is clear that for all conditions except for C1
 242 (overcast days) the agreement between model simulations (with both options) and observations is better at the T-Logger on
 243 the tongue (TL8, with a $RMSE = 1.03$ and $RMSE = 1.05$ for all conditions for GBvarH and GB98, respectively) than at

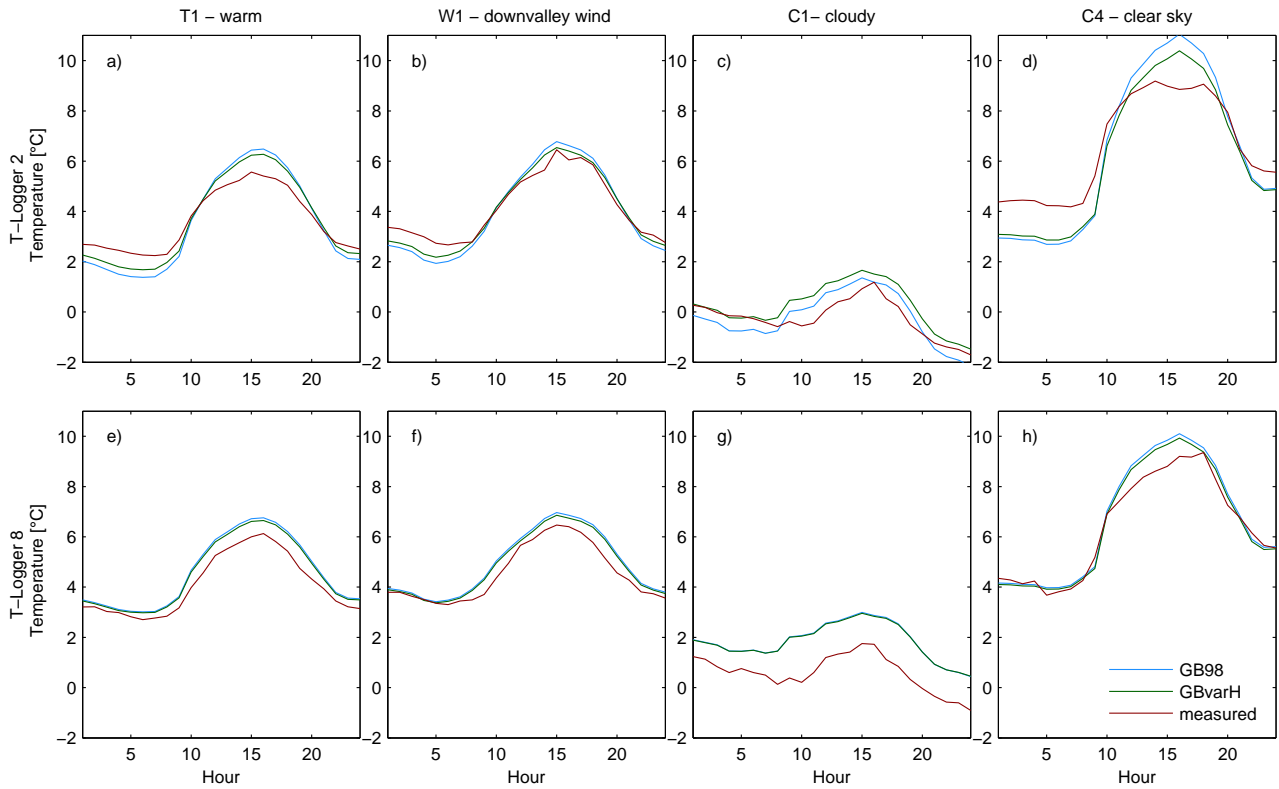


Fig. 6. Mean diurnal cycle of measured air temperature compared with the results of the unmodified model (GB98) and model with variable H (GBvarH) for selected climatic conditions (described in Table 2) at TL2 in the upper section and TL8 in the lower section of the glacier.

244 the one in the upper section of the glacier (TL2, with a $RMSE = 1.09$ and $RMSE = 1.21$ for all conditions for GBvarH and
 245 GB98, respectively). This is mainly due to the underestimation of temperature in the early morning and late evening by the
 246 model compared to the observation at TL2 (Figure 6a, b and d), while this effect is no longer visible at TL8 (Figure 6e, f
 247 and h). It is also evident that while no difference in model performance can be observed between the two model versions at
 248 TL2, the model with variable H (GBvarH) works slightly better at the lower T-Logger. Under cloudy, cold conditions, the fit
 249 between modelled and observed average temperatures is poorer for both models especially at TL8 (Figure 6c and g).

250 6. DISCUSSION AND CONCLUSIONS

251 The along-glacier temperature distribution at HGdA is poorly represented by a constant linear LR. On the upper glacier, above
 252 about 2900 m a.s.l., the LR is typically weak and often positive, indicating a shallow boundary layer and strong temperature
 253 stratification in the lowest few m of the atmosphere. Below 2900 m a.s.l. on the glacier tongue, LRs are highly variable but
 254 frequently strongly negative particularly when katabatic winds develop. Averaged over the entire glacier over the period of
 255 measurement the mean LR is shallower than the ELR. Use of a constant LR calibrated with local data improves the fit to

256 observed temperature and results in a reduced RMSE. It should be kept in mind, however, that a large amount of data was
257 used to derive the CLRcal and these might not be commonly available. The two methods tested as alternative to a constant LR,
258 GB98 and GBvarH, reduce the RMSE further. The GB98 model in its unmodified form over- or underestimates temperature
259 at most locations and conditions, whereas the GBvarH better captures the shape of the temperature profile along the flowline
260 for most of the weather cases considered, even though an overestimation is still evident. Hence, the assumption of a constant
261 thickness of the glacier boundary layer does not seem to hold for HGdA. The variability in H was also stated by various authors
262 and partly ascribed to the larger fetch for katabatic winds towards the tongue of the glacier (e.g. Strasser and others, 2004;
263 Shea and Moore, 2010). The correspondence of mainly downvalley winds (W1) with high temperature agrees with the general
264 prerequisite of a high temperature deficit favoring the development of katabatic wind (e.g. Ohata, 1989; Greuell and others,
265 1997; Klok and others, 2005; Pellicciotti and others, 2008; Shea and Moore, 2010). Under such conditions the GB98 model
266 would be expected to work best, as the main requirements, the presence of a glacier wind and temperatures higher than 0°C ,
267 are fulfilled (see Greuell and Böhm, 1998). For clear sky days (C4), as well as partly cloudy days (C3), the better performance
268 of GBvarH on the lower part of the glacier corresponds with the better development of katabatic winds further down on the
269 glacier due to topographic constraints (e.g. Strasser and others, 2004; Shea and Moore, 2010), such as the narrowing towards
270 the tongue. High radiation on sunny and clear sky days (C3 and C4) produces warm ambient air that is cooled by the ice
271 surface (Stenning and others, 1981), and the strong adiabatic warming on the lower part of the tongue is well captured by
272 the GBvarH model. In contrast, the poor performance on cloudy days (C1), when temperatures are overestimated for most
273 of the glacier, might be due to the fact that the solar warming process is reduced by the presence of clouds, and the lower
274 temperature deficit prevents the development of katabatic flows, a prerequisite of the model (Greuell and Böhm, 1998). A
275 possible reason for the poor performance of GB98, especially on the tongue, might be local effects. The influence of warming
276 from surrounding slopes and debris patches could be an additional explanation for the steep increase in temperature at TL9,
277 but it is impossible to test such hypotheses without more data. It is also difficult to envisage the processes whereby warm
278 air over the moraines can be transferred to the T-Logger stations, as heat advection would require cross-glacier wind which
279 does not seem to occur on the tongue. The other process that could be responsible for such warming is longwave radiation
280 emission. At the glacier tongue the valley narrows to about 500 m width so that emission from the snow-free slopes might be
281 more important than in the upper section. This effect, however, is difficult to quantify and seems to be small according to a
282 study by Juszak and Pellicciotti (2012). It is difficult to identify the main reasons for the observed temperature variability with
283 the limited amount of data available and our study clearly points to the need to improve our understanding of temperature
284 variability over glaciers. For a quantification of these local effects the number of measurement sites should be expanded.

285 The conclusion that GBvarH works better than the original model means that we need a variable L_R (length scale) in
286 the model which can be due to an actual variability in H along the glacier flowline or to a variable c_H . The validity of the
287 assumption that c_H is constant should be investigated by full energy balance calculations, while more knowledge should be
288 gained on the actual height of the GBL as well as its variability in space and main controls.

289 Some studies have found katabatic wind acceleration at night following radiative cooling (Manins and Sawford, 1979; Horst
290 and Doran, 1986). The model is able to capture this possible behavior in the lower part of the glacier, but underestimates
291 temperature in the upper part (see Figure 6). This again suggests a strong temperature stratification in the lowest few m of the
292 atmosphere in the upper part of the glacier, where the boundary atmospheric layer is poorly developed due to a short fetch.
293 Under such conditions, the 2 m measurement height is likely to be outside of the 'constant flux layer' where the atmosphere is
294 fully adjusted to the underlying surface, and a basic assumption of most energy-balance melt models will not be met in any
295 case. As above, only more data on the height and characteristics of the GBL can provide a clear explanation for the observed
296 variability at night.

297 The main conclusions of this study are that:

298 The GB98 model is an improvement over the assumption of a constant LR, even when locally calibrated, as demonstrated
299 by a reduction in the RMSE.

300 For HGdA, the model works better when different glacier boundary layer thicknesses, H , are used for different sections of
301 the glacier, as it captures the shape of the along-glacier temperature distribution and replicates the actual temperatures
302 better.

303 The model works better for clear sky conditions and high temperatures as the greater temperature deficit typical of these
304 cases favors the development of a katabatic wind, which commonly occurs under sunny summer conditions.

305 The model does not work well for cloudy conditions.

306 It is also apparent from our results that no readily applicable model exists to derive distributed temperature field over a
307 glacier, nor any can be developed without additional measurements sheading light on the height and characteristics of the
308 KBL.

309 Overall, the performance of GB98 is found to be acceptable under conditions and locations where a katabatic wind can de-
310 velop, and represents an improvement over the use of a constant LR. However, different models for air temperature distribution
311 are needed: in areas where the fetch is short or gradients are shallow; under cool and/or cloudy conditions; and when synoptic

312 forcing of the wind dominates. Our results provide evidence for a possible variability of the height of the GBL that should be
313 supported by experimental evidence. Our measurements are inadequate to investigate the height and structure of the GBL,
314 which would require tower measurements at different heights. Our results, however, seem to clearly call for an increase of such
315 experiments and should give inputs for this sort of investigation. The finding that better results can be obtained by allowing
316 the height of the GBL to vary long the glacier flowline should be tested for other sites.

317 In this work we compared four options for modelling air temperature with respect to their ability to reproduce the observed
318 temperatures. Differences are evident but are in some cases small. The effect that each method would have on the magnitude
319 of simulated melt and mass balance should also be evaluated.

320 GB98 and GBvarH can partly explain the low sensitivity of GBL temperature to external atmospheric temperature changes,
321 and so help address an important challenge in estimating glacier response to climatic changes. Successful application of the
322 model requires knowledge of the initiation point for katabatic flows, however, and this would probably require local calibration
323 data in most cases. Supported by new field data, future research should focus on incorporating different physical conditions
324 and topographic effects in order to develop a model able to reproduce realistic temperature data time-series throughout the
325 glacier which would be a milestone achievement for melt modelling in general.

326 7. ACKNOWLEDGEMENTS

327 The authors would like to thank all the people involved in the field campaign 2010: Andreas Bauder, Cyrill Buergi, Ilaria
328 Clemenzi, Jacopo Sanfilippo, Jakob Helbing, Lea Mueller, Luca Salvatore, Luzia Sturzenegger, Markus Konz, Martin Heynen,
329 Maurizio Savina, Mauro Bruno, Roger Bordoy Molina, Tim Reid. Thomy Keller helped us build the structure for the T-Loggers.
330 The authors are grateful to Prof. Paolo Burlando for supporting MC and the field campaign on HGdA.

331 References

- 332 Arnold, N. S., W. G. Rees, A. J. Hodson and J. Kohler, 2006. Topographic controls on the surface energy balance of a high
333 Arctic valley glacier, *Journal of Geophysical Research*, **111**(F2), F02011.
- 334 Arnold, N. S., I. C. Willis, M. J. Sharp, K. S. Richards and W. J. Lawson, 1996. A distributed surface energy–balance model
335 for a small valley glacier. I. Development and testing for Haut Glacier d’Arolla, Valais, Switzerland, *Journal of Glaciology*,
336 **42**(140), 77–89.
- 337 Braithwaite, R. J., Y. Zhang and S. C. B. Raper, 2002. Temperature sensitivity of the mass balance of mountain glaciers and
338 ice caps as a climatological characteristic, *Zeitschrift für Gletscherkunde und Glazialgeologie*, **1**, 35–61.
- 339 Brock, B., C. Mihalcea, M. Kirkbride, G. Diolaiuti, M. Cutler and C. Smiraglia, 2010. Meteorology and surface energy fluxes
340 in 2005–2007 ablation seasons at Miage debris-covered glacier, Mont Blanc Massif, Italian Alps, *Journal of Geophysical*

- 341 *Research*, **115**(D9), D09106.
- 342 Brock, B. W. and N. S. Arnold, 2000. A spreadsheet-based (Microsoft Excel) point surface energy balance model for glacier
343 and snow melt studies, *Earth Surface Processes and Landforms*, **25**(6), 649–658.
- 344 Brock, B. W., I. C. Willis and M. J. Sharp, 2006. Measurement and parameterization of aerodynamic roughness length
345 variations at Haut Glacier d’Arolla, Switzerland, *Journal of Glaciology*, **52**(177), 281–297.
- 346 Brutsaert, W., 1975. On a derivable formula for long-wave radiation from clear skies, *Water Resources Research*, **11**(5),
347 742–744.
- 348 Carenzo, M., F. Pellicciotti, S. Rimkus and P. Burlando, 2009. Assessing the transferability and robustness of an enhanced
349 temperature-index glacier-melt model, *Journal of Glaciology*, **55**(190), 258–274.
- 350 Chutko, K. J. and S. F. Lamoureux, 2009. The influence of low-level thermal inversions on estimated melt-season characteristics
351 in the central Canadian Arctic, *International Journal of Climatology*, **29**(2), 259–268.
- 352 Farinotti, D., S. Usselman, M. Huss, A. Bauder and M. Funk, 2012. Runoff evolution in the Swiss Alps: projections for
353 selected high-alpine catchments based on ENSEMBLES scenarios, *Hydrological Processes*, **26**(13), 1909–1924.
- 354 Gardner, A. S. and M. Sharp, 2009. Sensitivity of net mass-balance estimates to near-surface temperature lapse rates when
355 employing the degree-day method to estimate glacier melt, *Annals of Glaciology*, **50**(50), 80–86.
- 356 Gardner, A. S., M. J. Sharp, R. M. Koerner, C. Labine, S. Boon, S. J. Marshall, D. O. Burgess and D. Lewis, 2009. Near-Surface
357 Temperature Lapse Rates over Arctic Glaciers and Their Implications for Temperature Downscaling, *Journal of Climate*,
358 **22**(16), 4281–4298.
- 359 Greuell, W and R. Böhm, 1998. 2 m temperatures along melting mid-latitude glaciers, and implications for the sensitivity of
360 the mass balance to variations in temperature, *Journal of Glaciology*, **44**(146), 9–20.
- 361 Greuell, W., W. H. Knap and P. C. Smeets, 1997. Elevational changes in meteorological variables along a midlatitude glacier
362 during summer, *Journal of Geophysical Research*, **102**(D22), 25941–25954.
- 363 Hock, R. and B. Holmgren, 2005. A distributed surface energy-balance model for complex topography and its application to
364 Storglaciären, Sweden, *Journal of Glaciology*, **51**(172), 25–36.
- 365 Horst, T. W. and J. C. Doran, 1986. Nocturnal drainage flow on simple slopes, *Boundary-Layer Meteorology*, **34**(3), 263–286.
- 366 Hulth, J., C. Rolstad, K. Trondsen and R. Wedøe Rødby, 2010. Surface mass and energy balance of Sørbreen, Jan Meyen,
367 2008, *Annals of Glaciology*, **51**(55), 110–119.
- 368 Huss, M., A. Bauder, M. Funk and R. Hock, 2008. Determination of the seasonal mass balance of four Alpine glaciers since
369 1865, *Journal of Geophysical Research*, **113**(F1), F01015.

- 370 Juszak, I. and F. Pellicciotti, 2012. A comparison of parameterisations of incoming longwave radiation over melting glaciers:
371 model robustness and seasonal variability, in revision (JGR).
- 372 Klok, E. J., M. Nolan and M. R. Van den Broeke, 2005. Analysis of meteorological data and the surface energy balance of
373 McCall Glacier, Alaska, USA, *Journal of Glaciology*, **51**(174), 451–461.
- 374 Klok, E. J. and J. Oerlemans, 2002. Model study of the spatial distribution of the energy and mass balance of Morter-
375 atschgletscher, Switzerland, *Journal of Glaciology*, **48**(163), 505–518.
- 376 Li, X. and M. W. Williams, 2008. Snowmelt runoff modelling in an arid mountain watershed, Tarim Basin, China, *Hydrological*
377 *Processes*, **22**(19), 3931–3940, doi:10.1002/hyp.7098.
- 378 Machguth, H., F. Paul, M. Hoelzle and W. Haeberli, 2006. Distributed glacier mass-balance modelling as an important
379 component of modern multi-level glacier monitoring, *Annals of Glaciology*, **43**(1), 335–343.
- 380 Manins, P. C. and B. L. Sawford, 1979. A model of katabatic wind, *Journal of Atmospheric Science*, **36**(4), 619–630.
- 381 Marshall, S. J. and M. J. Sharp, 2008. Temperature and Melt Modeling on the Prince of Wales Ice Field, Canadian High
382 Arctic, *Journal of Climate*, **22**, 1454–1468.
- 383 Marshall, S. J., M. J. Sharp, D. O. Burgess and F. S. Anslow, 2007. Near-surface-temperature lapse rates on the Prince of
384 Wales Icefield, Ellesmere Island, Canada: implications for regional downscaling of temperature, *International Journal of*
385 *Climatology*, **27**(3), 385–398.
- 386 Marty, C. and R. Philipona, 2000. The clear-sky index to separate clear-sky from cloudy-sky situations in climate research,
387 *Geophysical Research Letters*, **27**(17), 2649–2652.
- 388 Michlmayr, G., M. Lehning, G. Koboltschnig, H. Holzmann, M. Zappa, R. Mott and W. Schner, 2008. Application of the
389 Alpine 3D model for glacier mass balance and glacier runoff studies at Goldbergkees, Austria, *Hydrological Processes*,
390 **22**(19), 3941–3949, doi: 10.1002/hyp.7102.
- 391 Minder, J. R., P. W. Mote and J. D. Lundquist, 2010. Surface temperature lapse rates over complex terrain: Lessons from the
392 Cascade Mountains, *Journal of Geophysical Research*, **115**(D14), D14122.
- 393 Nienow, P., M. Sharp and I. Willis, 1996. Temporal Switching between Englacial and Subglacial Drainage Pathways: Dye
394 Tracer Evidence from the Haut Glacier d’Arolla, Switzerland, *Geografiska Annaler. Series A, Physical Geography*, **78**(1),
395 51–60.
- 396 Nolin, A. W., J. Phillippe, A. Jefferson and S. L. Lewis, 2010. Present-day and future contributions of glacier runoff to
397 summertime flows in a Pacific Northwest watershed: Implications for water resources, *Water Resources Research*, **46**(W12),
398 W12509.

- 399 Ohata, T., 1989. Katabatic wind on melting snow and ice surfaces (I.) Stationary wind on a large maritime glacier, *Journal*
400 *of the Meteorological Society of Japan*, **67**, 99–112.
- 401 Paul, F., H. Escher-Vetter and H. Machguth, 2009. Comparison of mass balances for Vernagtferner, Oetzal Alps, as obtained
402 from direct measurements and distributed modeling, *Annals of Glaciology*, **50**(50), 169–177.
- 403 Pellicciotti, F., B. Brock, U. Strasser, P. Burlando, M. Funk and J. Corripio, 2005. An enhanced temperature-index glacier
404 melt model including the shortwave radiation balance: development and testing for Haut Glacier d’Arolla, Switzerland,
405 *Journal of Glaciology*, **51**(175), 573–587.
- 406 Pellicciotti, F., J. Helbing, A. Rivera, V. Favier, J. Corripio, J. Araos, J.-E. Sicart and M. Carenzo, 2008. A study of the
407 energy balance and melt regime on Juncal Norte Glacier, semi-arid Andes of central Chile, using melt models of different
408 complexity, *Hydrological Processes*, **22**(19), 3980–3997.
- 409 Pepin, N. and M. Losleben, 2002. Climate change in the Colorado Rocky Mountains: Free air versus surface temperature
410 trends, *International Journal of Climatology*, **22**(3), 311–329.
- 411 Petersen, L. and F. Pellicciotti, 2011. Spatial and temporal variability of air temperature on a melting glacier: Atmospheric
412 controls, extrapolation methods and their effect on melt modeling, Juncal Norte Glacier, Chile, *Journal of Geophysical*
413 *Research*, **116**(D23), D23109.
- 414 Shea, J. M. and R. D. Moore, 2010. Prediction of spatially distributed regional-scale fields of air temperature and vapor
415 pressure over mountain glaciers, *Journal of Geophysical Research*, **115**(D23), D23107.
- 416 Stahl, J., R. D. Moore, J. A. Floyer, M.G. Asplin and I.G. McKendry, 2006. Comparison of approaches for spatial interpolation
417 of daily air temperature in a large region with complex topography and highly variable station density, *Agricultural and*
418 *Forest Meteorology*, **139**(3–4), 224–236.
- 419 Stenning, A. J., C. E. Banfield and G. J. Young, 1981. Synoptic controls over katabatic layer characteristics above a melting
420 glacier, *International Journal of Climatology*, **1**(4), 309–324.
- 421 Strasser, U., J. Corripio, F. Pellicciotti, P. Burlando, B. Brock and M. Funk, 2004. Spatial and temporal variability of meteo-
422 rological variables at Haut Glacier d’Arolla (Switzerland) during the ablation season 2001: Measurements and simulations,
423 *Journal of Geophysical Research*, **109**(D3), D03103.
- 424 Stull, R.B., 1988. An introduction to boundary layer meteorology, Springer.
- 425 van den Broeke, M. R., 1997. Structure and diurnal variation of the atmospheric boundary layer over a mid-latitude glacier
426 in summer, *Boundary-Layer Meteorology*, **83**(2), 183–205.
- 427 Willis, I., N. Arnold and B. Brock, 2002. Effect of snowpack removal on energy balance, melt and runoff in a small supraglacial
428 catchment, *Hydrological Processes*, **16**(14), 2721–2749.